The FASEB Journal

RESEARCH ARTICLE OPEN ACCESS

Low-Intensity Pulsed Ultrasound Promotes Osteogenesis in Porous Titanium Alloys Through miR-1187/BMP4 Pathway

Limei Qin | Hongjuan Cao | Xiaohan Liu | Di Zhang | Lin Wu

Department of Prosthodontics, School of Stomatology, China Medical University, Shenyang, China

Correspondence: Lin Wu (wulin13@163.com)

Received: 26 December 2024 | **Revised:** 4 April 2025 | **Accepted:** 18 April 2025

Funding: This work was supported by National Natural Science Foundation of China (Grants 81801807 and 81870811) and National Natural Science Foundation of Liaoning Province (Grant 2020-BS-110).

Keywords: BMP4 | LIPUS | miR-1187 | osteogenesis

ABSTRACT

The repair of critical-sized bone defects remains a significant clinical challenge. Low-intensity pulsed ultrasound (LIPUS), in combination with porous titanium alloy (PTi) scaffolds, has emerged as a promising therapeutic strategy. However, its molecular mechanism remains unclear. This study aimed to investigate the role of bone morphogenetic protein 4 (BMP4) and microRNA-1187 (miR-1187) in LIPUS-mediated osteogenesis in PTi scaffolds. In vitro, the expression of BMP4 and miR-1187 in MC3T3-E1 cells following LIPUS stimulation was assessed using quantitative real-time PCR (RT-qPCR), western blotting, ELISA, alkaline phosphatase (ALP) activity assay, and staining techniques. A luciferase reporter assay confirmed BMP4 as a direct target of miR-1187. Functional studies demonstrated that BMP4 overexpression and miR-1187 inhibition promoted osteoblast differentiation, whereas BMP4 knockdown and miR-1187 overexpression suppressed osteogenesis. In vivo, a BMP4 knockdown rat model was established by si-BMP4 injection into mandibular defects and evaluated new bone formation using micro-CT and histological analyses. LIPUS stimulation significantly upregulated BMP4 expression, promoted new bone formation in PTi scaffolds, and partially rescued the inhibitory effects of BMP4 silencing. These findings establish BMP4 as a key regulator in LIPUS-enhanced osteogenesis via miR-1187 suppression. This mechanistic insight supports the combined use of LIPUS and PTi scaffolds for bone defect repair and highlights BMP4 as a potential therapeutic target to further enhance bone regeneration in LIPUS-stimulated scaffold therapies.

1 | Introduction

The healing of critical-sized bone defects presents a persistent clinical challenge. Autografts and allografts, the traditional approaches for bone repair, have limitations for treating critical-sized bone defects, including limited donor sources, potential donor site complications, and risks of immune rejection. Consequently, significant research has focused on developing effective artificial bone substitutes. Porous titanium alloys (PTi), produced via 3D printing, offer excellent biocompatibility, robust corrosion resistance, high mechanical strength, low Young's modulus, and a well-organized porous structure, making them highly suitable for surgical bone substitutes [1, 2]. However, the biological inertness of titanium alloys limits their osteogenic effectiveness [3]. Thus, researchers have investigated various approaches, including surface modifications [4–6] and

Limei Qin, Hongjuan Cao, and Xiaohan Liu contributed equally to this study.

biophysical interventions [7, 8] to enhance the bioactivity of titanium alloys. Among these, noninvasive biophysical interventions have shown promise for promoting osteogenesis [7, 8].

Low-intensity pulsed ultrasound (LIPUS) is a noninvasive mechanical wave therapy shown to accelerate the healing of fractures and bone defects [9]. LIPUS stimulation effectively promoted human osteosarcoma cell proliferation and osteogenic differentiation in porous Ti6Al4V alloy [10] and bone marrow mesenchymal stem cells (BMSCs) adhesion and differentiation on titanium surfaces [11]. The US Food and Drug Administration has approved LIPUS for treating nonunion fractures and accelerating fracture healing [7, 8]. Numerous studies confirm that LIPUS promotes bone healing [9, 10], making its combination with bone scaffolds a promising new strategy for treating critical-sized bone defects [11, 12]. Our previous work demonstrated that LIPUS promotes the migration and osteogenic differentiation of osteoblasts within PTi scaffolds, as well as bone tissue growth and bone maturation within scaffolds [13, 14]. However, LIPUS stimulation alone does not guarantee uniform bone growth throughout the porous material. In particular, bone formation in the middle regions of the scaffolds remains insufficient. Therefore, to advance the clinical translation of LIPUS-PTi for critical-sized bone defect repair, it is essential to further investigate the underlying biological mechanisms.

MicroRNAs (miRNAs) have recently been identified as regulatory mechanisms influencing the expression of mRNAs and proteins. Through base-pairing with partially or fully complementary sequences on target mRNAs, miRNAs play crucial roles in the differentiation of osteoblasts [15]. Here, we investigated changes in miRNAs associated with the combined application of LIPUS [16, 17] and PTi. Our miRNA profiling data of LIPUS-irradiated MC3T3-E1 cells on PTi identified 30 significantly downregulated miRNAs. Among these, miR-1187 showed more than a tenfold downregulation. Limited studies have explored miR-1187's regulatory involvement in hepatocyte apoptosis [18], early diabetic nephropathy [19], traumatic arthritis [20], and osteogenesis [15], suggesting it may also play a role in bone formation.

Studies have shown that miRNAs can regulate bone morphogenetic proteins (BMPs), critical growth factors for bone and cartilage formation and maturation. First identified by Professor Urist for their ability to induce ectopic bone formation, BMPs are now recognized as pivotal in skeletal development [21]. Our bioinformatics analysis identified BMP4 as a potential target gene of miR-1187. As a prominent member of the BMP family with high osteogenic activity, BMP4 plays key roles in stem cell maintenance and differentiation [22–24]. While BMPs have been shown to promote osteogenic differentiation [25, 26], their specific involvement in LIPUS-induced osteogenesis, particularly within porous implant materials, remains underexplored. This study investigated whether BMP4 plays a role in LIPUS-mediated osteogenesis within PTi scaffolds.

Thus, the aim of this study was to determine whether LIPUS regulates PTi osteogenesis by modulating the miR-1187/BMP4 axis, providing a theoretical foundation for potential therapeutic applications of LIPUS-stimulated PTi scaffolds combined with BMP4-targeted therapy for bone defect repair.

2 | Materials and Methods

2.1 | MC3T3-E1 Cell Culture

MC3T3-E1 cells were cultured in alpha-minimum essential medium (α-MEM, HyClone, USA) supplemented with 10% fetal bovine serum (FBS, TianHang Biotech, Zhejiang, China) at 37°C with 5% CO_2. The complete medium was replaced every two days, and cells were subcultured upon reaching 85% confluency via trypsinization.

The porous scaffolds (10 mm diameter, 3 mm height, 400–500 μm pore size, 65%–70% porosity) were vacuumed and prewetted for 4 h before cell seeding. A total of 1×10^4 MC3T3-E1 cells in 20 μL suspension were seeded onto each scaffold and incubated for 2 h to allow initial attachment. Subsequently, 2 mL of complete medium was added to each well, and the seeded scaffolds were incubated for an additional 24 h to ensure firm adhesion. The scaffolds were then randomly assigned to either the LIPUS irradiation group or the sham irradiation control group.

2.2 | LIPUS Stimulation

LIPUS stimulation was performed in a water bath using a Sonicator 740 (Mettler Electronics Corp., CA, USA), following previously established protocols [1]. LIPUS stimulation parameters were set as follows: frequency, 1 MHz; intensity, 40 mW/cm^2; pulse duration, 1 ms; exposure time, 20 min per day. The sham irradiation control group underwent identical procedures without ultrasound activation.

2.3 | Experimental Animals

Forty-eight male Sprague Dawley (SD) rats (290–320 g, 8–10 weeks old) were obtained from Huafukang Co., LTD (Beijing, China) and housed in a specific pathogen-free (SPF) laboratory under laminar airflow conditions at the Animal Experiment Center of China Medical University. The rats underwent mandibular segmental defect surgery with scaffold implantation and were randomly assigned to one of four groups: control + PBS group, LIPUS + PBS group, control + si-BMP4 group. Each group was further subdivided into two time points (4 and 8 weeks post-operation), with six rats per time point. All experiments adhered to the guiding principles of the Guide for the Care and Use of Laboratory Animals [27], and were approved by the Animal Ethics Committee of China Medical University (authorization ethics number: CMU2021259).

2.4 | Surgical Procedure

Following a one-week acclimatization period, rats underwent surgery under anesthesia induced via intraperitoneal injection of 3% sodium pentobarbital (0.15–0.2 mL/100 g; Wokai, Shanghai, China). The mandibular region was shaved, disinfected with iodophor, and injected subcutaneously with 0.5 mL of 1% lidocaine for local anesthesia. A rectangular mandibular

defect (6 × 4 × 2 mm) was created using a dental handpiece fitted with a sterile burr (MZ-06, Wincore Power Tools, China), as previously described [28]. During drilling, sterile saline was used for irrigation to prevent thermal damage. The porous titanium scaffold (Pti) was press-fitted into the defect site, and the incision was carefully sutured in layers. Postoperatively, benzylpenicillin sodium (80 000 IU; TIANWUDR, Tianjin, China) was administered for three days to prevent infection.

Three days post-surgery, the rats were subjected to LIPUS irradiation or local drug injection under isoflurane anesthesia. For the Control+si-BMP4 and LIPUS+si-BMP4 groups, 100 μL of si-BMP4 (5 nmol) was injected into the Pti scaffold, while an equivalent volume of PBS was injected for the Control+PBS and LIPUS+PBS.

2.5 | Fluorochrome Labeling and Euthanasia

To assess active bone formation, calcein green (10 mg/kg) and xylenol orange (90 mg/kg) were administered intraperitoneally at 10 and 3 days before euthanasia, respectively. At 4 and 8 weeks post-intervention, rats were euthanized using isoflurane followed by CO_2 overdose. Mandibles were harvested, dissected to remove soft tissues, and stored in either liquid nitrogen or 4% paraformaldehyde for subsequent analysis.

2.6 | Transfection Assay

The experiment was repeated 3 times.

BMP4 siRNA (si-BMP4), negative control siRNA (si-NC), miR-1187 mimics, miR-1187 inhibitor, and corresponding negative controls were synthesized by GenePharma (Suzhou, China). Overexpression plasmids (pcDNA3.1-BMP4) and control vectors (pcDNA3.1) were obtained from Syngen (Beijing, China). Transfections were performed using Lipofectamine 3000 (Invitrogen, USA) in Opti-MEM I Reduced Serum Medium (Invitrogen, USA), following the manufacturer's protocol. Final concentrations for transfection were as follows: si-BMP4, miR-1187 mimics, and si-NC: 50 nM; miR-1187 inhibitor and inhibitor NC: 100 nM; pcDNA3.1-BMP4 and pcDNA3.1: 1 μg. Experiments were performed in triplicate.

2.7 | RNA Extraction and RT-qPCR

Total RNA was extracted from cultured cells and bone tissues using RNAiso Plus Reagent (Takara, Japan) and the EASYspin Plus Bone Tissue Rapid Extraction Kit (Aidlab, China), respectively. cDNA synthesis for mRNA and miRNA was performed using the PrimeScript RT reagent Kit (Takara, Japan) and Mir-X miRNA First-Strand Synthesis Kit (Takara, Japan). Quantitative real-time PCR (RT-qPCR) was conducted using a 7500 Real-Time PCR system (ABI, USA) with TB Green Premix Ex Taq II (Takara, Japan). Gene expression was normalized to GAPDH (mRNA) or U6 (miRNA) using the $2^{-\Delta\Delta Ct}$ method. Experiments were performed in triplicate. All the primers were synthesized by Sangon Biotech (Shanghai, China).

2.8 | Western Blot Analysis

MC3TE-E1 cells were lysed with RIPA mixed buffer containing 98.9% RIPA (50 mM Tris) (pH 7.4), 150 mM NaCl, 1% Triton X-100, 1% sodium deoxycholate, 0.1% SDS, along with various inhibitors including sodium orthovanadate, sodium fluoride, EDTA, and leupeptin, 1% protease inhibitor cocktail, and 0.1% Benzonase Nuclease. Total protein concentrations were determined by BCA assay (Beyotime, China). Equal amounts of protein (30 μg) were subjected to 10% SDS-PAGE and transferred to PVDF membranes (Millipore, USA). Membranes were blocked with 5% non-fat milk for 1.5 h and incubated overnight at 4°C with primary antibodies. Following washes, membranes were incubated with HRP-conjugated secondary antibodies, and signals were detected using an enhanced chemiluminescence kit (Tanon, China). Densitometric analysis was performed using ImageJ software. The following antibodies were used for this study: ALP, 1:1000, Abcam (ab108337); COL-1, 1:1000, Abcam (ab34710); BMP4, 1:1000, Abcam (ab39973); RUNX2, 1:250, Santa Cruz (sc390351); GAPDH, 1:6000, Proteintech (60004-1-lg), anti-rabbit IgG (1:10 000), Proteintech (SA00001-1) and anti-mouse IgG (1:10 000), Proteintech (SA00001-1). Experiments were conducted in triplicate.

2.9 | ELISA Assay

Supernatants were collected 72 h post-transfection with miR-1187 mimics, miR-1187 inhibitor, or after LIPUS irradiation. BMP4 protein levels in the supernatant were quantified using a mouse BMP-4 ELISA kit (EK0316, Boster, China) following the manufacturer's protocol. Briefly, 100 μL of standard diluent and samples were added to each well of the ELISA plate and incubated at 37°C for 90 min. Subsequently, 100 μL of biotinylated anti-mouse BMP4 antibody working solution was added, followed by incubation at 37°C for 60 min.

After three washes, 100 μL of avidin-peroxidase complex working solution was added and incubated at 37°C for 30 min. The plate was washed five times before adding 90 μL of TMB substrate and incubating at 37°C for 15–20 min in the dark. The reaction was stopped by adding 100 μL of stop solution, and absorbance was measured at 450 nm. BMP4 content in the samples was calculated based on the standard curve generated using the reference standard. Experiments were conducted in triplicate.

2.10 | ALP Activity Assay

ALP activity was measured by following previously published protocols [13, 14]. Briefly, after 7 days of co-culturing, the cells were lysed using 0.3% Triton-100; then they were centrifuged at 12 000 rpm for 5 min. The supernatant was collected for ALP activity measurement using the ALP Activity Assay Kit (A059-2-2, JianCheng, China), with absorbance read at 560 nm. The total protein concentration in the supernatant was determined using a BCA assay (Beyotime, China). ALP activity was calculated using the following formula: ALP (U/gprot) = [(absorbance of the measuring tube − absorbance of the blank control)/(absorbance of the

standard tube—absorbance of the blank control) × amount of phenol in the standard tube (0.02 mg)]/amount of total protein in each sample (g). Experiments were conducted in triplicate.

2.11 | ALP Staining

After 10 days of co-culturing, the cells were washed three times with PBS and fixed in 4% paraformaldehyde for 20 min at room temperature. The fixed cells were then stained using the Alkaline Phosphatase Substrate Kit (C3206, Beyotime, China) according to the manufacturer's protocol. The images of stained specimens were taken. Experiments were conducted in triplicate.

2.12 | Mineralization Assay

After 10 days of co-culturing, the cells were washed three times with PBS and fixed in 4% paraformaldehyde for 20 min at room temperature. The fixed cells were stained using the Alizarin Red S Staining Kit for Osteogenesis (C0148S, Beyotime, China) according to the manufacturer's protocol. The images of stained specimens were captured.

For quantitative analysis of Alizarin Red S staining, 1 mL of 10% cetylpyridinium chloride was added to each well and incubated with shaking for 30 min. The dissolved mineralized matrix was transferred to a 96-well plate (150 μL per well), and absorbance was measured at 560 nm. Experiments were conducted in triplicate.

2.13 | Luciferase Reporter Assay

The 3′UTR region of BMP4, containing either wild-type (WT) or mutant (MUT) miRNA binding sites, was synthesized and cloned into the pmirGLO vector (GenePharma, China). Cells were seeded into 96-well plates and co-transfected with 400 ng of pmirGLO-BMP4 3′UTR (WT), pmirGLO-BMP4 3′UTR (MUT), or an empty pmirGLO vector, along with 50 nM miR-1187 mimics or mimics NC, using Lipofectamine 3000. Cells were harvested 48 h post-transfection, and luciferase activity was measured using the Dual-Luciferase Reporter Assay System (Promega, USA) following the manufacturer's protocol. Each experiment was repeated three times.

2.14 | Micro-CT Evaluation

After fixation in paraformaldehyde for one-week, three-dimensional quantitative images of the harvested mandibles were obtained using a micro-computed tomography (Micro-CT) system (SkyScan1276, Bruker, Germany). Scans were performed along the scaffold's long axis with a resolution of 10 μm, a source voltage of 70 kV, and a current of 200 μA. Three-dimensional images were reconstructed and analyzed using image analysis software (DataViewer, CTAn, CTvox, Bruker, Germany). The region of interest (ROI) was defined as a rectangular area matching the defect dimensions. Gray-scale values above 180 were classified as scaffold material, while values between 70 and 180 were identified as new bone tissue. The percentage of bone ingrowth within the scaffold was calculated using the pore occupancy fraction (POF): POF = Vbone/(V_{bone} + $V_{residual\ pore}$) × 100% [13].

2.15 | Preparation of Non-Decalcified Sections

After μ-CT scanning, the specimens were processed to make non-decalcified sections as described in previous studies [13, 14]. Briefly, specimens were rinsed under running water for 24 h to remove residual paraformaldehyde, dehydrated in a graded ethanol series (70%, 80%, 90%, 95%, and 100%), and embedded in methyl methacrylate. Sections (60 μm thick) were cut using a Leica-SP 1600 diamond-saw microtome (Wetzlar, Germany). Two middle sections per sample were selected and numbered to ensure comparability.

2.16 | Fluorescence Microscopy Analysis

Calcein-xylenol orange double-labeled sections were directly observed under a fluorescence microscope (Olympus BX 51 + DP71, Japan). Calcein was excited at 450–480 nm, while xylenol orange was excited at 510–560 nm. The different fluorescence signals indicated bone apposition at different time points. The mineral apposition rate (MAR) was measured as the distance between the two fluorescence bands using Image-Pro Plus 6.0 software and calculated using the equation [13, 14]: MAR = distances of double fluorescence labeling/time.

2.17 | Toluidine Blue (TB) Staining

Sections were stained with TB working solution (G3668, Solarbio, China) at room temperature following the manufacturer's protocol. Stained sections were observed under a light microscope (Olympus BX 51 + DP71, Japan). Bone area (A_{bone}) and total pore area ($A_{residual\ pore}$) were quantitatively analyzed using Image-Pro Plus 6.0 software, and the percentage of newly formed bone was calculated as follows: percentage of de novo bone = $A_{bone}/A_{bone} + A_{residual\ pore}$ [13].

2.18 | Von Kossa Staining

Von Kossa staining was performed according to the manufacturer's protocol (G3282, Solarbio, China), followed by counterstaining with Van Gieson solution (Solarbio, China). Bone tissue was stained red, while mineralized deposits appeared dark brown. Histological evaluation was performed using light microscopy, and mineralized deposits were quantitatively analyzed using Image-Pro Plus 6.0 software by calculating the integrated optical density (IOD) of the black-brown deposits.

2.19 | Statistical Analysis

Statistical analysis was performed using SPSS Statistics 23.0 (IBM, USA). Data normality was confirmed using the

Shapiro–Wilk test. Results are presented as mean ± standard deviation (SD). Statistical comparisons were analyzed using Student's *t*-test (two groups), one-way or two-way ANOVA, followed by Tukey's post hoc test (multiple groups). Differences with $p < 0.05$ were considered statistically significant.

3 | Results

3.1 | LIPUS Positively Regulates Osteogenic Differentiation in MC3T3-E1

After 7 days of co-culture with scaffolds, MC3T3-E1 cells were analyzed using RT-qPCR and western blot to assess intracellular mRNA and protein expression levels. The mRNA expression level of *Col-1*, *Alp*, *Runx2*, and *Ocn* as well as the protein expression level of COL-1, ALP, and RUNX2 were detected. As shown in Figure 1A,B, compared with the control group, LIPUS irradiation promoted the gene expression levels of *Col-1*, *Alp*, *Runx2*, and *Ocn* as well as the protein expression levels of COL-1, ALP, and RUNX2, indicating that LIPUS positively regulated osteogenic differentiation in MC3T3-E1, which was in consist with our previous study [13, 14].

3.2 | Identification of Differential Expression miRNAs During LIPUS-Induced Osteogenic Differentiation

To investigate miRNA expression changes during LIPUS-induced osteogenic differentiation, we performed miRNA high-throughput sequencing on osteoblasts cultured on scaffolds with or without LIPUS irradiation. The miRNA profiling data revealed that LIPUS significantly downregulated 30 miRNAs, with miR-1187 exhibiting a more than tenfold decrease (Figure 2A). However, no significantly upregulated miRNAs were observed. These findings were further validated by RT-qPCR, which confirmed the downregulation of several miRNAs under LIPUS irradiation, with miR-1187 displaying the most obvious reduction (Figure 2B), consistent with the sequencing results.

3.3 | MiR-1187 Negatively Regulates Osteogenic Differentiation in MC3T3-E1

To assess the role of miR-1187 in osteogenic differentiation, MC3T3-E1 cells were transfected with 50 nM of miR-1187 mimics or mimics NC, or 100 nM of miR-1187 inhibitor or inhibitor NC, according to the experimental groups. RT-qPCR confirmed that miR-1187 expression was significantly upregulated in cells transfected with miR-1187 mimics (Figure 2C). Furthermore, miR-1187 overexpression suppressed the expression of osteogenic marker genes, including *Col-1*, *Alp*, *Runx2*, and *Ocn* (Figure 2D). Western blot analysis further demonstrated that miR-1187 mimics downregulated the protein expression levels of COL-1, ALP, and RUNX2 (Figure 2E), while this inhibitory effect was reversed in miR-1187 inhibitor-transfected cells (Figure 2F). ALP activity assays revealed a significant reduction in ALP levels in miR-1187 mimics-transfected cells compared to the NC group, whereas this effect was attenuated by miR-1187 inhibition (Figure 2H). Consistently, ALP staining at day 10 post-transfection showed similar results (Figure 2G). Additionally, the impact of miR-1187 on mineralized nodule formation was evaluated via Alizarin Red S staining. miR-1187 overexpression reduced mineralized nodule formation after 21 days of culture, whereas miR-1187 inhibition promoted mineralization (Figure 2I). The semiquantitative analysis of mineralization further demonstrated that the OD value was highest in the miR-1187 inhibitor group, followed by the control group, with the lowest value observed in the miR-1187 mimics group. Moreover, compared with the LIPUS group, miR-30c-1-3p mimics with LIPUS irradiation decreased the gene and protein expression levels of osteogenic markers(Figure 2J–L). These findings indicate that miR-1187 negatively regulates osteogenic differentiation in MC3T3-E1 cells by downregulating osteogenic gene and protein expression, inhibiting ALP activity, and suppressing mineralized matrix formation under LIPUS irradiation.

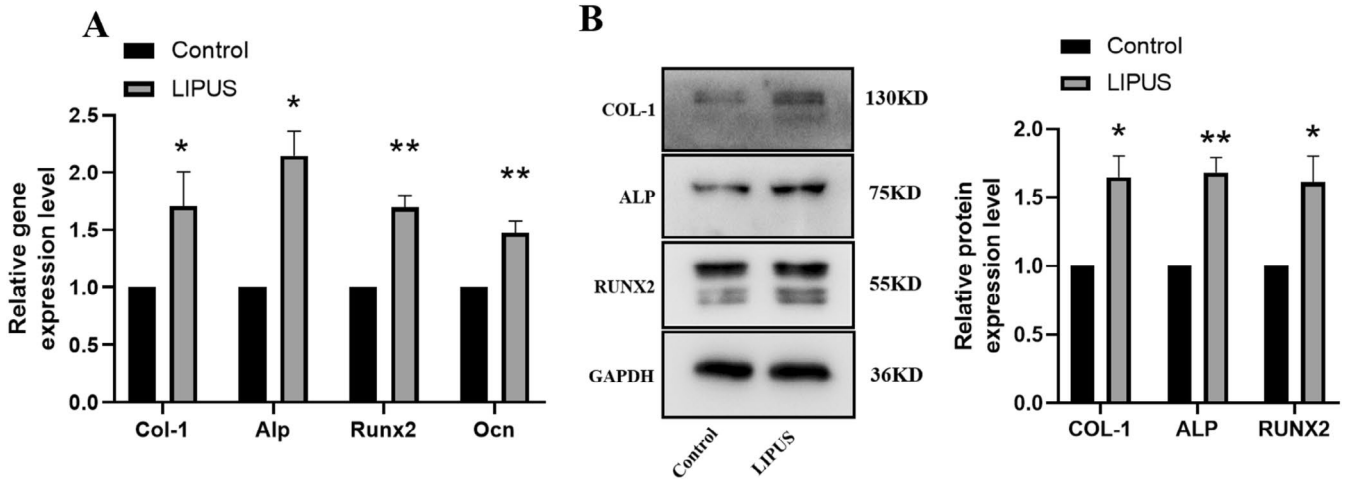

FIGURE 1 | LIPUS positively regulated osteogenic differentiation in MC3T3-E1. (A) Effect of daily LIPUS irradiation on mRNA expression of *Col-1, Alp, Runx2*, and *Ocn*. (B) Effect of daily LIPUS irradiation on protein expression of COL-1, ALP, and RUNX2. All values represent means ± SD ($n = 3$). *$p < 0.05$, **$p < 0.01$ compared with the control.

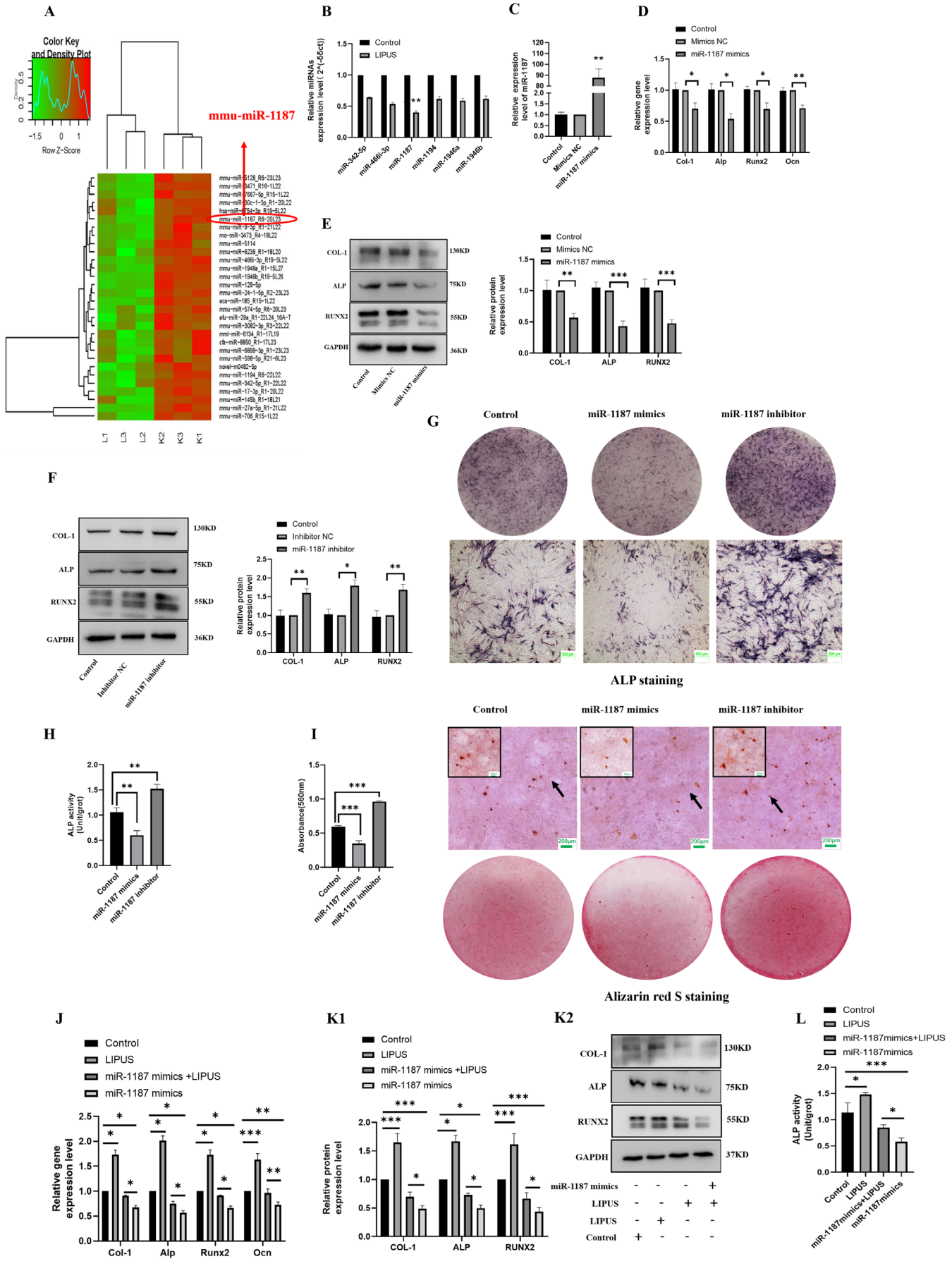

FIGURE 2 | Legend on next page.

FIGURE 2 | LIPUS significantly downregulated the expression of miR-1187 and miR-1187 negatively regulates osteogenic differentiation in MC3T3-E1. (A) miRNA array expression profiling. LIPUS significantly down-regulate the expression of 30 miRNAs. L: LIPUS, K: Control. (B) miR-1187 expression was significantly downregulated after daily LIPUS irradiation of 7 days. (C) qRT-PCR analysis confirmed the transfection efficiency of miR-1187 mimics. (D) qRT-PCR analysis. mRNA expression of osteoblast marker genes including Col-1, Alp, Runx2, and Ocn were significantly downregulated in miR-1187 mimics-transfected group. (E) Western blot analysis for osteogenesis-related proteins COL-1, ALP, RUNX2 at 72 h after transfection with miR-1187 mimics. (F) Western blot analysis for osteogenesis-related proteins COL-1, ALP, RUNX2 at 72 h after transfection with miR-1187 inhibitor. (G) ALP staining on day 10 in miR-1187 mimics and inhibitor-transfected MC3T3-E1cells (scale bar = 500 μm). (H) ALP activity detection on day 7 in miR-1187 mimics and inhibitor-transfected MC3T3-E1cells. (I) Alizarin red S staining and quantitative analysis of Alizarin Red S accumulation on day 21 in miR-1187 mimics and inhibitor-transfected MC3T3-E1cells (scale bar = 200 μm/100 μm), the black arrow indicate the magnified area, the magnified pictures were marked within the square frame in the image. All values represent means ± SD ($n = 3$). Effects of miR-1187 mimics on the expression of osteogenic markers under LIPUS irradiation: qRT-PCR analysis(J), western blot (K1) and quantitative analysis (K2), ALP activity(L). *$p < 0.05$, **$p < 0.01$, ***$p < 0.001$.

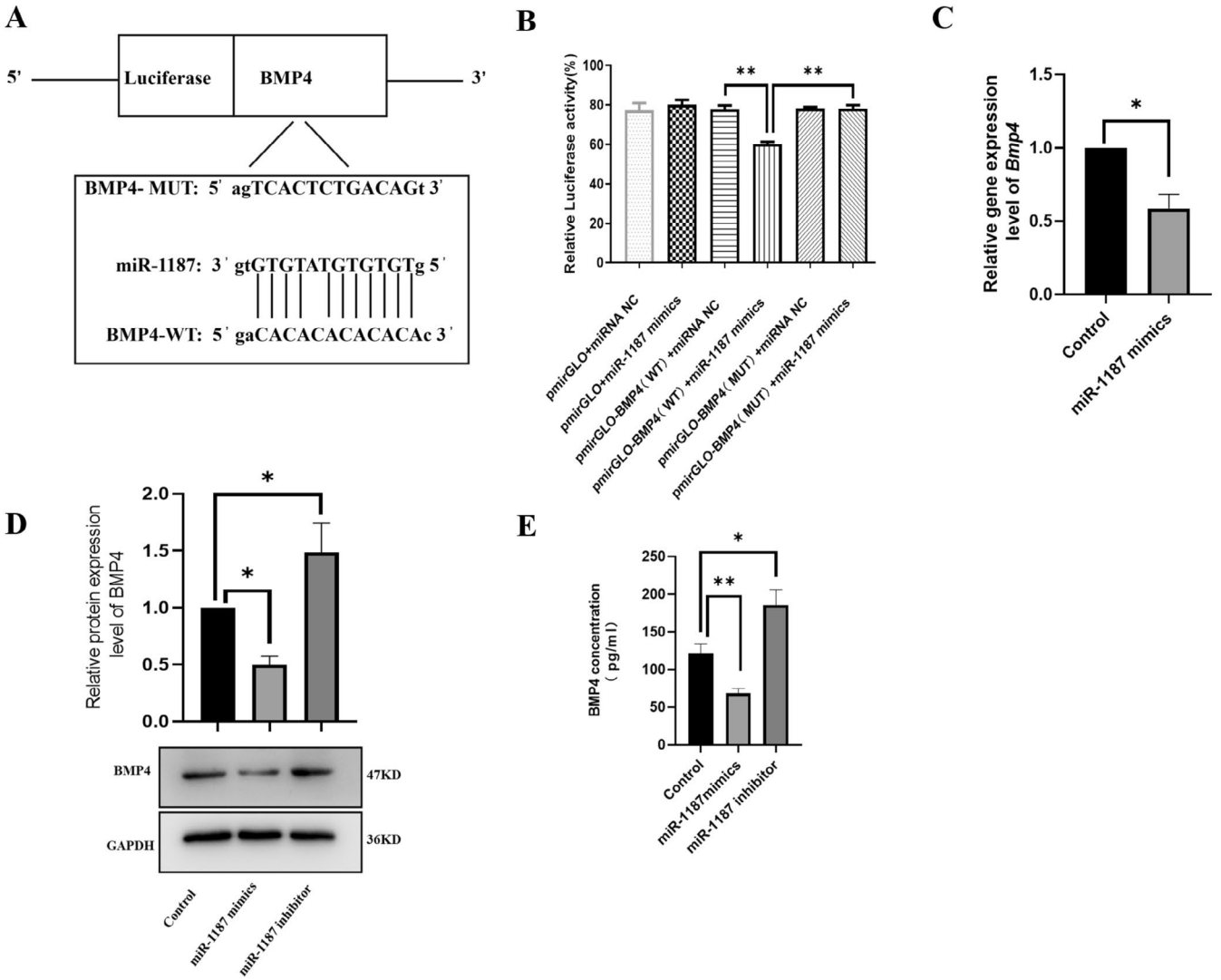

FIGURE 3 | miR-1187 directly targets BMP4. (A) The predicted binding site between miR-1187 and BMP4 by bioinformatics analysis. (B) The luciferase activity of the BMP4-WT and BMP4-MUT in MC3T3-E1 cells treated with miR-1187 mimics or NC. (C) mRNA expression of Bmp4 was significantly downregulated in the miR-1187 mimics-transfected group. (D) Western blot analysis for the expression of BMP4 protein in miR-1187 mimics and inhibitor-transfected MC3T3-E1 cells on Pti. (E) ELISA assay analysis for the expression of supernatant BMP4 secreted protein in miR-1187 mimics and inhibitor-transfected MC3T3-E1cells on Pti. All values represent means ± SD.($n = 3$). *$p < 0.05$, **$p < 0.01$.

3.4 | MiR-1187 Directly Targets BMP4

To elucidate the molecular mechanism by which miR-1187 regulates osteogenic differentiation in MC3T3-E1 cells, target prediction tools miRWalk and RNAhybrid were employed to identify potential miR-1187 target genes. Among the many potential genes, BMP-4, a member of the TGF-β superfamily which has a major role in osteogenesis, brought our attention. The

predicted binding sequence between miR-1187 and the 3′UTR of BMP4 is shown in Figure 3A. To validate this interaction, luciferase reporter constructs containing either the wild-type BMP4 3′UTR (BMP4-WT) or a mutated binding site (BMP4-MUT) were generated. The luciferase reporter assay revealed a significant decrease in luciferase activity in the BMP4-WT group upon miR-1187 overexpression, while no significant change was observed in the BMP4-MUT group (Figure 3B). These results indicate that miR-1187 specifically binds to the predicted site within the BMP4 3′UTR.

To further investigate the regulatory relationship between miR-1187 and BMP4, MC3T3-E1 cells were transfected with miR-1187 mimics or inhibitors. RT-qPCR demonstrated that miR-1187 overexpression significantly reduced *bmp4* mRNA levels compared to the control group (Figure 3C). Consistently, ELISA and Western blot analyses showed decreased BMP4 protein expression following miR-1187 mimic transfection, whereas this inhibitory effect was reversed in miR-1187 inhibitor-transfected cells (Figure 3D,E).

These findings collectively demonstrate that miR-1187 negatively regulates BMP4 expression at both mRNA and protein levels by directly targeting its 3′UTR.

3.5 | BMP4 Positively Regulates Osteogenic Differentiation in MC3T3-E1

To investigate the role of BMP4 in regulating osteogenic differentiation of MC3T3-E1 cells, a *bmp4* knockdown model was established by transfecting cells with three different siRNAs. RT-qPCR analysis demonstrated that all three si-BMP4 sequences significantly reduced *bmp4* mRNA expression, with si-BMP4_785 exhibiting the most effective silencing (Figure 4A). Consequently, si-BMP4_785 was selected for subsequent experiments. The efficiency of BMP4 overexpression was similarly validated via RT-qPCR (Figure 4B). Both RT-qPCR and Western blot analyses revealed that BMP4 knockdown significantly downregulated, while BMP4 overexpression markedly upregulated, the gene and protein expression levels of key osteogenic differentiation markers (Figure 4C–F). The osteogenic phenotype was further assessed through ALP activity, ALP staining, and Alizarin Red S staining. As shown in Figure 4G–I, BMP4 knockdown reduced ALP activity and staining, whereas BMP4 overexpression enhanced both. Moreover, matrix mineralization, as confirmed by Alizarin Red S staining and quantitative analysis, exhibited a similar trend. Collectively, these results indicate that BMP4 plays a positive regulatory role in promoting osteogenic differentiation in MC3T3-E1 cells.

3.6 | LIPUS Promotes MC3T3-E1 Differentiation by Inhibiting miR-1187 Targeted Upregulation of BMP4

The expression of BMP4 in MC3T3-E1 cells cultured on Pti scaffolds, with or without LIPUS irradiation, was analyzed. The results showed that LIPUS significantly upregulated BMP4 expression at both the mRNA and protein levels (Figure 5A–C). Furthermore, the expression of osteogenesis-related markers was markedly downregulated in the si-BMP4 group compared to the control, and the expression of osteogenesis-related markers was markedly downregulated in the si-BMP4 group with LIPUS irradiation compared to the LIPUS group. However, in the si-BMP4 + LIPUS group, these markers were notably increased relative to the si-BMP4 group (Figure 5D,E). In addition, the si-BMP4 group with LIPUS irradiation decreased ALP activity compared to the LIPUS group; LIPUS treatment mitigated the reduction in ALP activity induced by si-BMP4 transfection (Figure 5F). These findings indicate that LIPUS irradiation can rescue the suppression of osteogenic differentiation caused by BMP4 silencing, suggesting that LIPUS regulates BMP4 expression to enhance osteogenesis in MC3T3-E1 cells.

To explore the regulatory mechanism by which LIPUS interacts with miR-1187, overexpression models of miR-1187 and BMP4 were established in MC3T3-E1 cells. Consistent with previous results, transfection with miR-1187 mimics significantly downregulated BMP4 and osteogenesis-related markers at both the mRNA (Figure 5G) and protein levels (Figure 5I), as well as reduced ALP activity (Figure 5H), compared to the control group. In contrast, co-transfection with miR-1187 mimics and a BMP4 overexpression plasmid restored the expression of osteogenesis-related markers and ALP activity relative to the miR-1187 mimic group. Similarly, the LIPUS+miR-1187 mimics group exhibited elevated levels of these indicators compared to the miR-1187 mimics group (Figure 5G–I).

3.7 | RT-qPCR of De Novo Bone

To investigate the function of BMP4 in vivo, we performed an experiment in four groups of male SD rats. The study plan was shown in Figure 4A. Real-time PCR analysis of the de novo bone showed that the *Bmp4* mRNA level was significantly lower in the si-BMP4 group compared with the control group at both 4 weeks and 8 weeks, while LIPUS irradiation significantly promoted the *Bmp4* mRNA level (Figure 6B1), indicating that the in vivo model of BMP4 knockdown was successfully constructed and LIPUS irradiation could upregulate the *Bmp4* mRNA level in vivo.

As shown in Figure 6B1,B2, mRNA expression levels of *Col-1*, *Runx2*, *Alp*, and *Ocn* were significantly elevated in the LIPUS-treated group but decreased in the si-BMP4-treated group at various time points compared to the control. In addition, the expression levels of these osteogenic gene markers were significantly lower in the si-BMP4 + LIPUS group compared to the LIPUS-irradiated group, but they were significantly higher when compared to the si-BMP4-treated group. These results indicate that BMP4 knockdown suppresses, whereas LIPUS irradiation enhances, the expression of osteogenic gene markers. Moreover, LIPUS treatment partially alleviated the inhibitory effects of si-BMP4 on gene expression.

3.8 | Micro-CT Images and Fluorescence Double Labeling

Three-dimensional reconstruction of scaffolds and de novo bone was performed by CTvox software. The 3D images showed that

de novo bone volume increased with time in all four groups; the volume of de novo bone was higher in the LIPUS group than in the control group, but lower in the si-BMP4 group than in the control group (Figure 6C1). Quantitative analysis of the micro-CT data further demonstrated that the POF significantly decreased in the si-BMP4-treated group, whereas it increased with LIPUS irradiation. Importantly, the POF value in the si-BMP4 + LIPUS group was elevated compared to the si-BMP4 group but remained lower than the LIPUS group (Figure 6C2), indicating that LIPUS mitigated the bone loss associated with BMP4 knockdown.

Representative fluorescence double-labeling images of newly formed bone are shown in Figure 6D2. Calcein and xylenol orange were used to label mineralized bone formed over 10 days and 3 days before euthanasia, respectively. Across all groups,

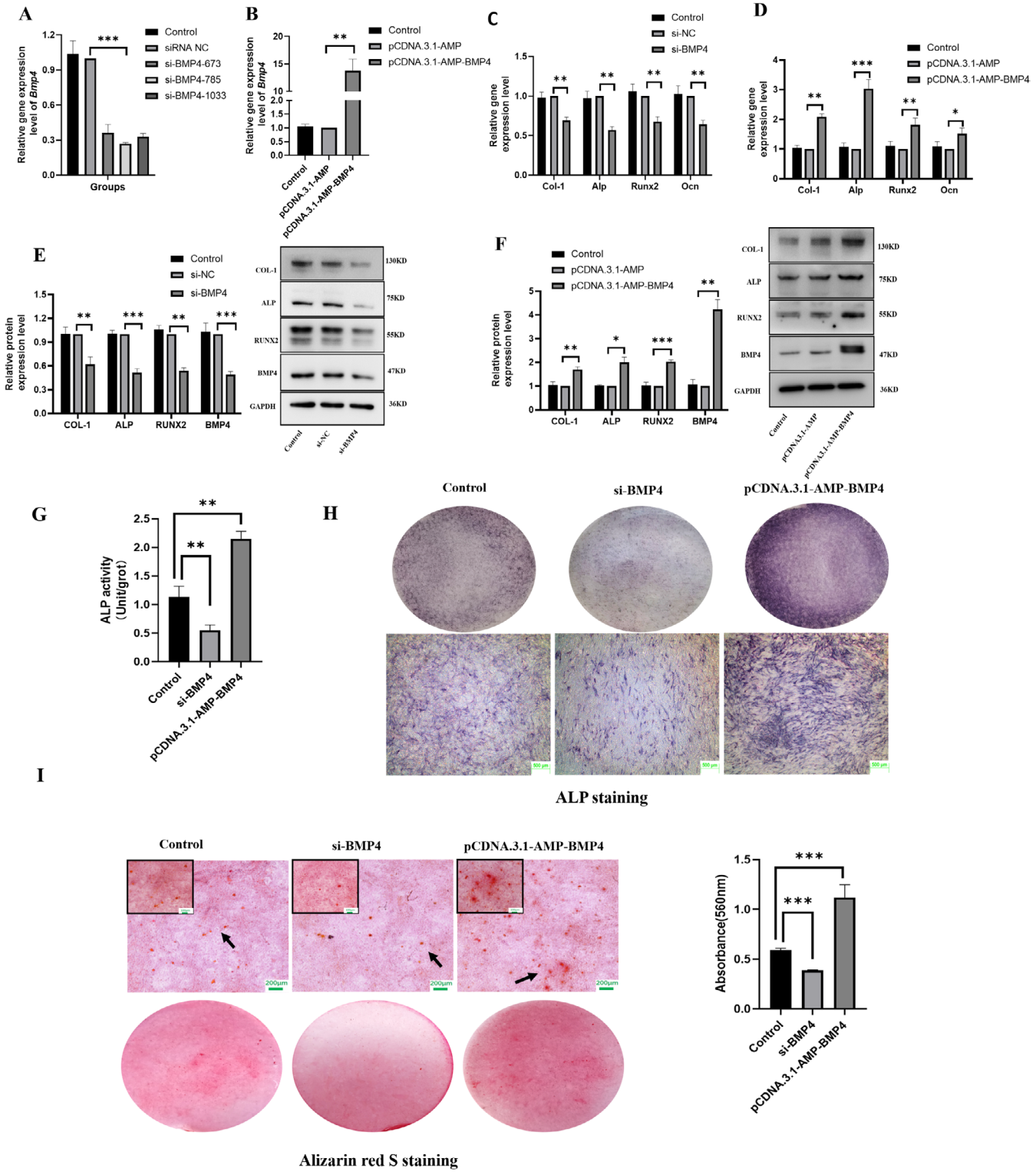

FIGURE 4 | Legend on next page.

FIGURE 4 | BMP4 positively regulates osteogenic differentiation in MC3T3-E1 cells. (A) Level of BMP4 decreased after transfected with different siRNA-BMP4, si-BMP4-785 was identified to have the highest transfection efficiency. (B) BMP4 transcript levels was determined by RT-PCR after transfected with overexpression plasmids of BMP4. (C) qRT-PCR analysis. Level of *Col-1*, *Alp*, *Runx2*, and *Ocn* mRNA expression was significantly downregulated in BMP4 silencing. (D) qRT-PCR analysis. Level of *Col-1*, *Alp*, *Runx2*, and *Ocn* mRNA expression was significantly upregulated in BMP4 overexpression. (E) Western blotting. Expression of BMP4 protein and osteogenesis-related proteins COL-1, ALP, RUNX2 as well as statistical analysis after transfecting si-BMP4. (F) Western blotting. Expression of BMP4 protein and osteogenesis-related proteins COL-1, ALP, RUNX2 as well as statistical analysis after transfecting pCDNA3.1-BMP4. (G) ALP activity detection on day 7 in si-BMP4 and pCDNA3.1-BMP4 transfected MC3T3-E1cells. (H) ALP staining on day 10 in si-BMP4 and pCDNA3.1-BMP4 transfected MC3T3-E1cells (scale bar = 500 μm). (I) Alizarin red S staining and quantitative analysis of Alizarin Red S accumulation on day 21 in si-BMP4 and pCDNA3.1-BMP4 transfected MC3T3-E1cells (scale bar = 200 μm/100 μm), the black arrow indicate the magnified area, the magnified pictures were marked within the square frame in the image. All values represent means ± SD ($n = 3$). *$p < 0.05$, **$p < 0.01$, ***$p < 0.001$.

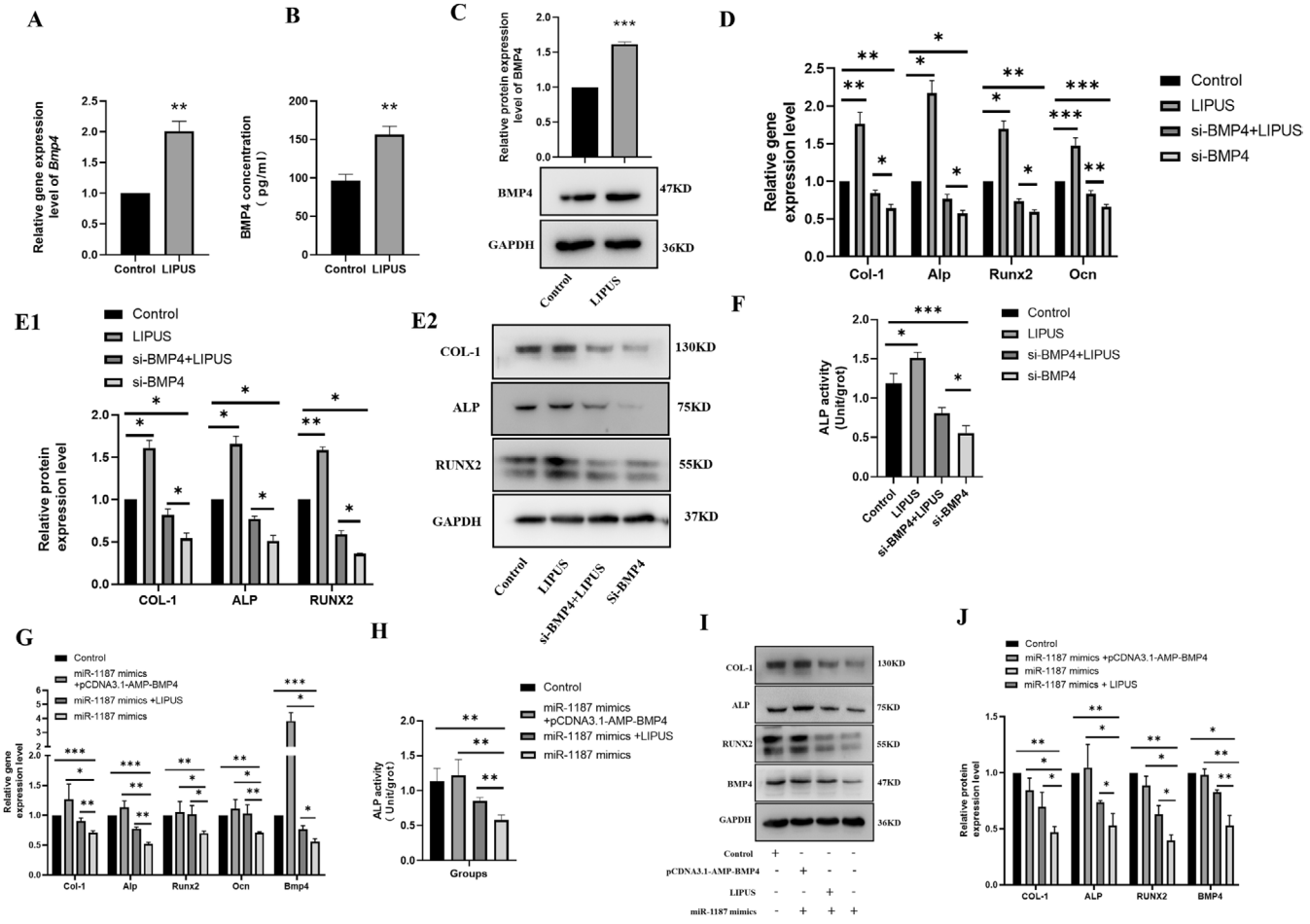

FIGURE 5 | LIPUS promotes osteogenic differentiation of MC3T3-E1 through inhibiting miR-1187 and upregulating BMP4. (A) qRT-PCR analysis. Effect of daily LIPUS stimulation on mRNA expression of Bmp4. (B) ELISA. Supernatant BMP4 secreted by cultured MC3T3-E1 cells was determined by ELISA assay. (C) Western blotting. BMP4 level was analyzed by western blot after 7 days LIPUS treatment. (D) Expression of osteogenesis-related mRNA was analyzed by qRT-PCR after si-BMP4 or si-bmp4 + LIPUS treatment. (E) Expression of osteogenesis-related protein was analyzed by western blot after si-BMP4 or si-BMP4 + LIPUS treatment. (F) ALP activity detection on day 7 in si-BMP4 and si-BMP4 + LIPUS-treated MC3T3-E1 cells. (G) Bmp4 and osteogenesis-related genes Col-1, Alp, Runx2, and Ocn expression in MC3T3-E1 cells on Pti as indicated treatment by qRT-PCR. (H) ALP activity in MC3T3-E1 cells on Pti on day 7 as indicated treatment. (I) Expression of BMP4 and osteogenesis-related proteins including COL-1, ALP, RUNX2 in MC3T3-E1 cells on Pti as indicated treatment by Western blot analysis. All values represent means ± SD ($n = 3$). Expression of osteogenesis-related protein was analyzed by western blot (E1) and quantitative analysis (E2) after si-BMP4, LIPUS or si-BMP4+LIPUS treated. Expression of BMP4 and osteogenesis- related proteins including COL- 1, ALP, RUNX2 in MC3T3- E1 cells on Pti as indicated treatment by Western blot analysis(I)andquantitative analysis (J). *$p < 0.05$, **$p < 0.01$, ***$p < 0.001$.

the mineral apposition rate (MAR) values declined over time from week 4 to week 8. However, the MAR of the si-BMP4 group was significantly lower than both the control and si-BMP4 + LIPUS groups at both time points. Conversely, the LIPUS group exhibited higher MAR values than the control and si-BMP4 + LIPUS groups (Figure 6D1). These findings confirm that LIPUS

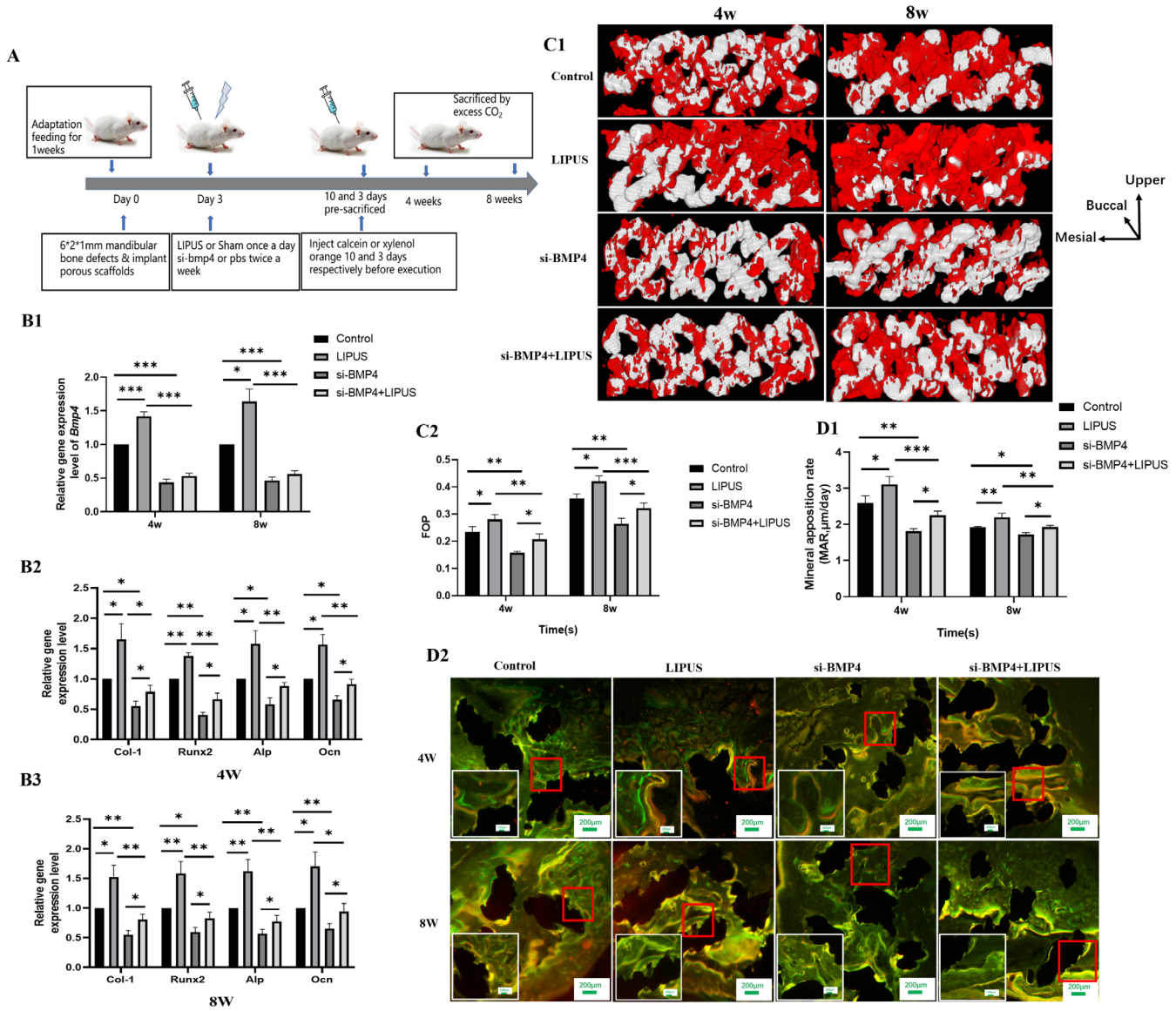

FIGURE 6 | LIPUS regulates bone formation in vivo. (A) Study plan of the vitro study. (B) qRT-PCR analysis of mRNA expression of Bmp4 as well as other osteogenesis-related gene in the de novo bone of different groups. B1: MRNA expression of Bmp4; B2, B3: Osteogenesis-related gene including Col-1, Alp, Runx2, and Ocn at 4 weeks and 8 weeks respectively. (C) Micro-CT analysis. C1: 3D reconstruction of the bone defect area at week 4 and 8. More bone ingrowth is observed as time increases in each group. The white part is the scaffold and the red part is the bone tissue. C2: The POF values for the Pti at 4 and 8 weeks. The POF values differ significantly between the LIPUS and control group, between the si-BMP4 and control group, as well as between the si-BMP4 and si-BMP4 + LIPUS group. (D) D1: The representative merged images of fluorescent double labeling of calcein(green color) and xylenol orange(orange color). The red square indicate the magnified area, the magnified pictures were marked within the white square frame in the image. (scale bar = 200 μm/100 μm). D2: The MAR of the four groups at 4 and 8 weeks. All values represent means ± SD ($n = 3$). *$p < 0.05$, **$p < 0.01$, ***$p < 0.001$.

irradiation enhances the mineralization rate of newly formed bone within porous scaffolds, particularly during the early stages of bone regeneration. In contrast, BMP4 knockdown impairs mineralization, though this effect can be partially reversed by LIPUS treatment.

3.9 | Histological Observation of the De Nova Bone

TB staining was performed to assess de novo bone formation, while Von Kossa staining was used to detect calcium salt deposition. As shown in Figure 7A, bone ingrowth increased over time. Initially, new bone was deposited adjacent to the host bone, gradually migrating to the center of the scaffold. In all groups, the visible pore area decreased, and the area of newly formed bone increased with time, with more de novo bone observed near the scaffold center. High-magnification images (200×) revealed that, at 4 weeks, cells in the new bone were disorganized, whereas, at 8 weeks, the bone tissue appeared more mature with cells arranged in a regular, lamellar pattern. Additionally, compared with the 4-week group, osteons—characteristic of mature bone—and more blood vessels were evident in the non-decalcified sections at 8 weeks. Figure 7B presents the quantitative analysis of bone formation

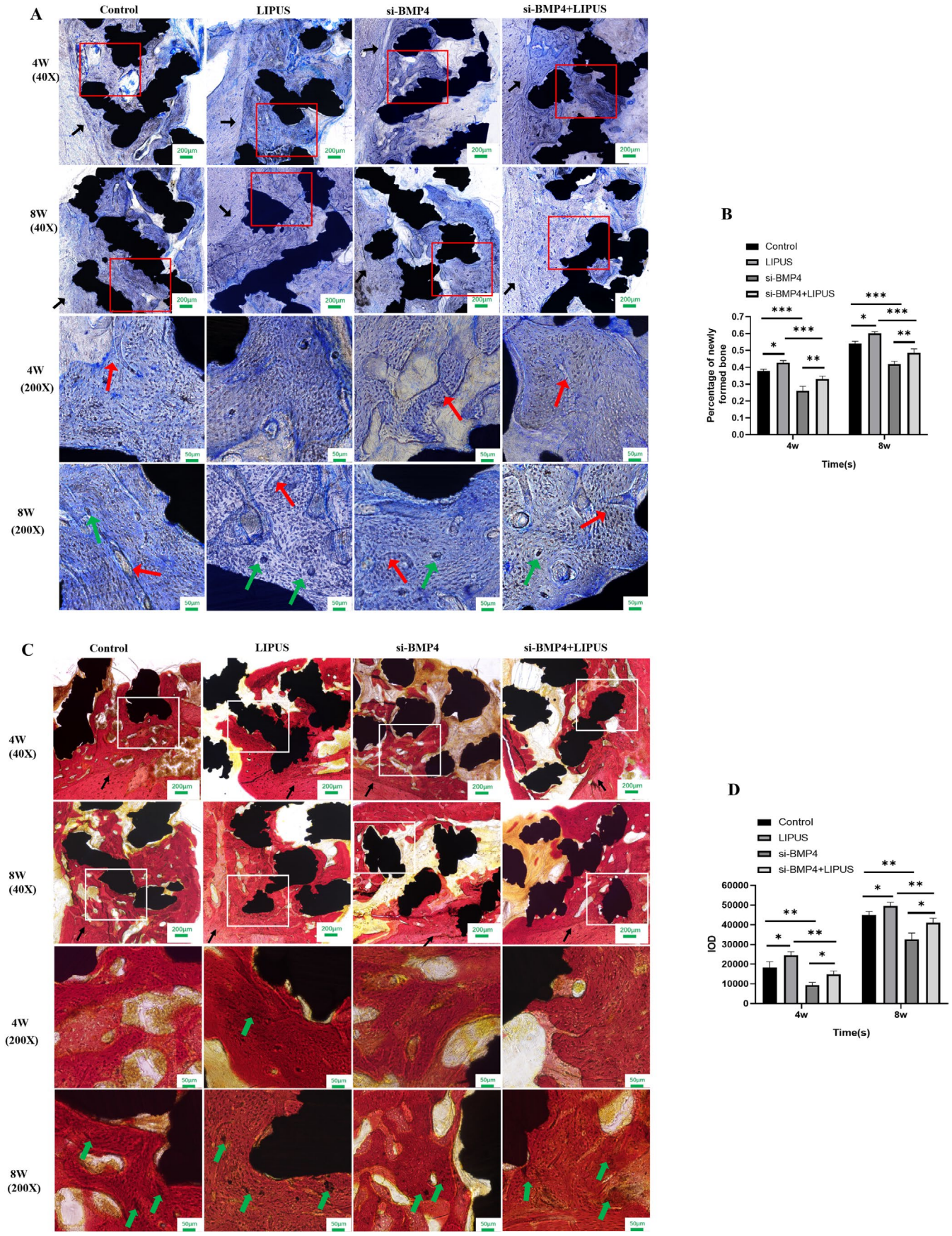

FIGURE 7 | Legend on next page.

FIGURE 7 | Histological staining of new bone tissue in vivo. (A) The representative histological images of non-decalcified sections obtained using TB staining. The black region is the Pti scaffold, the blue region is the bone tissue, the black arrows indicate the junction between the host bone and the de novo bone, the red arrows indicate neovascularization, the green arrows indicate the Haversian system. (scale bar = 200 μm/50 μm). (B) The percentages of the de novo bone formation in Pti calculated based on TB staining. (C) The representative histological images of non-decalcified sections obtained using von Kossa staining. The black region is the Pti scaffold, the red region is the bone tissue, the black arrows indicate the junction between the host bone and the de novo bone, while the green arrows indicate mineralized nodules (scale bar = 200 μm/50 μm). (D) The integrated optical density of the calcium salt deposition island of different groups at 4 and 8 week. All values represent means ± SD ($n = 3$). *$p < 0.05$, **$p < 0.01$, ***$p < 0.001$.

area percentage at different time points. Compared with the control group, the si-BMP4-treated group exhibited a significant reduction in bone formation area percentage at both 4 and 8 weeks, whereas the LIPUS-irradiated group showed a significant increase at both time points.

Representative Von Kossa staining images are shown in Figure 7C at both low and high magnifications. Low-magnification images indicated progressive scaffold space occupancy by newly formed bone across all groups. High-magnification views revealed fewer black-brown calcium salt deposits at 4 weeks, while more abundant and densely distributed deposits were observed at 8 weeks. The IOD values of calcium deposits (Figure 7D) demonstrated that bone maturity significantly increased over time in all groups. Notably, si-BMP4 treatment decreased calcium salt deposition, while LIPUS irradiation enhanced calcium deposition, promoting bone mineralization.

4 | Discussion

The noninvasive use of LIPUS offers clear advantages in clinical applications for bone defect repair. It has been confirmed that LIPUS enhances fracture healing at the tissue level in patients with a delayed union of the osteotomized fibula through an effect on the presence of RUNX2 immunopositive osteogenic cells [29]. Many studies have shown that LIPUS with a three-dimensional culture environment upregulates osteoblastic response [30, 31]. Our previous studies confirmed that LIPUS enhances differentiation of preosteoblast cell lines and new bone ingrowth within PTi scaffolds [13, 14]. However, the biological mechanisms by which LIPUS promotes osteogenesis in a three-dimensional material remain incompletely understood.

The role of miRNAs in stem cell or osteoblast differentiation is well documented, with numerous miRNAs implicated as essential regulators of osteogenesis [32]. Additionally, mechanical stimulation has been shown to modulate specific miRNAs [33]. To examine whether miRNAs contribute to the molecular regulation of LIPUS-promoted osteogenesis in 3D scaffolds, we analyzed miRNA profiling data and observed a significant downregulation of miR-1187 in LIPUS-stimulated MC3T3-E1 cells cultured on PTi. RT-PCR further validated this finding; functional assays using miR-1187 mimics and inhibitors demonstrated that miR-1187 acts as a negative regulator of osteogenesis. Specifically, miR-1187 inhibited the expression of osteogenesis-related factors such as Col-1, Runx2, Alp, and Ocn. Furthermore, miR-1187 decreased ALP activity and mineral nodule formation, while miR-1187 inhibition had the opposite effects. These results align with previous studies, confirming the negative regulatory role of miR-1187 in osteogenesis [15].

BMPs, particularly BMP-2, BMP-4, BMP-7, and BMP-9, are potent stimulators of osteogenic differentiation. Previous studies using 2D models of LIPUS stimulation suggest that LIPUS enhances osteogenic differentiation, possibly through BMP pathway activation. Daily LIPUS treatment significantly increased BMP-2, -4, and -7 and their receptors, and also phosphorylation of Smad1 expression of rat clonal cell line ROS 17/2.8 [25]. Nonetheless, BMP protein expression varies across different LIPUS stimulation models [26, 34]. Additionally, miRNAs modulated by BMP signaling are known to regulate BMP family members. For instance, miR-542-3p targets BMP-7 signaling and inhibits bone formation [16], miR-451a targets BMP-6 signaling [35], and miR-153 suppresses osteogenic differentiation by targeting BMPR-II [36]. In this study, BMP4 was identified as a candidate target gene through bioinformatic analysis. We subsequently investigated BMP4's role in LIPUS-promoted osteogenesis in PTi scaffolds and confirmed a regulatory relationship between miR-1187 and BMP4. Our dates showed that LIPUS stimulation significantly increased BMP4 expression in MC3T3-E1 cells on PTi. In vitro, BMP4 knockdown inhibited osteogenic differentiation, as evidenced by reduced expression of osteogenesis-related markers, decreased ALP activity, and lower mineral nodule formation. Conversely, BMP4 overexpression promoted osteogenic marker expression and enhanced ALP activity. These findings indicate that BMP4 positively regulates osteogenic differentiation in MC3T3-E1 cells. Moreover, LIPUS could mitigate the inhibitory effects of BMP4 silencing on osteogenesis.

To further clarify the relationship between miR-1187 and BMP4, we employed a dual-luciferase reporter assay, which confirmed that miR-1187 specifically binds to the 3′ untranslated region (UTR) of BMP4. We also observed that miR-1187 mimics decreased both BMP4 transcription and protein expression, whereas miR-1187 inhibition increased BMP4 protein levels. Co-transfection experiments showed that miR-1187 overexpression suppressed osteogenic markers and reduced ALP activity, while BMP4 overexpression reversed this suppression. Additionally, LIPUS counteracted the inhibitory effects of miR-1187 on osteogenesis. These results reveal that miR-1187 functions as a negative regulator of osteogenesis by repressing BMP4, while LIPUS promotes osteogenesis in PTi by upregulating BMP4 and downregulating miR-1187.

Bone tissue comprises various cellular components, collagen fibers, amorphous matrix organic material, and inorganic

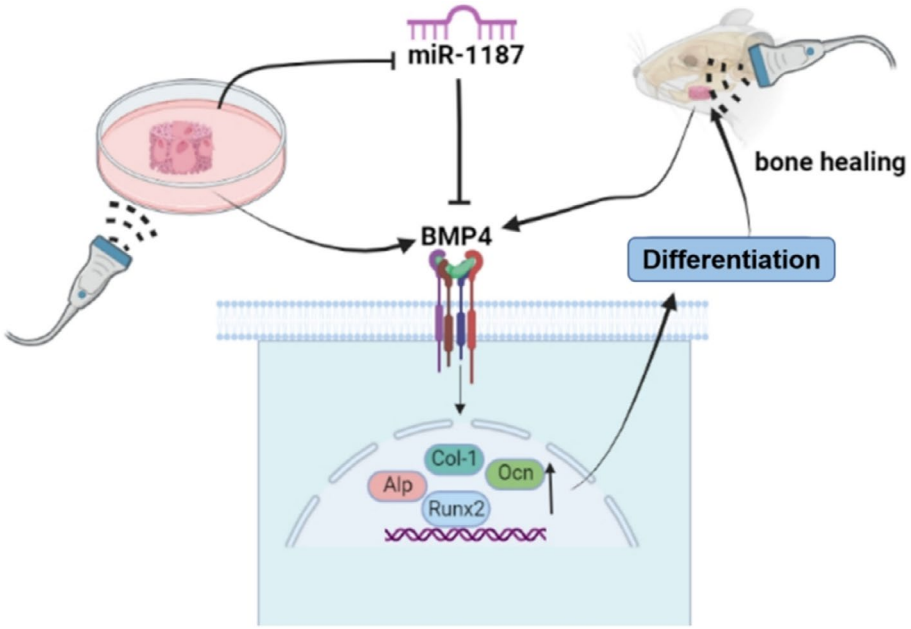

FIGURE 8 | The schematic of LIPUS promotes osteogenesis of porous titanium alloys through inhibiting miR-1187 and upregulating BMP4.

calcium salts. Manaka S, et al. reported that LIPUS increased the accumulation of inorganic phosphate and calcium in the extracellular matrix while upregulating the expression of bone ECM proteins [37]. Calcium salts are deposited on organic material, causing calcification and the formation of hardened bone, so the mineralization level in new bone reflects its maturity [38]. We constructed a BMP4 knockdown animal model via si-BMP4 injection and assessed the volume and maturity of new bone ingrowth using Micro-CT and histological analyses. LIPUS stimulation significantly increased bone volume, maturity, BMP4 expression, and osteogenic markers. Additionally, LIPUS-promoted bone formation by increasing femoral wet weight and trabecular bone mass in ovariectomized rats [39]. Volarić D, et al. created a critical-size bone defect (CSBD) model in rat calvaria to compare the effect of LIPUS and the autologous bone on bone healing. The results confirmed that LIPUS could represent a viable alternative to autologous bone grafts for repairing bone defects undergoing intramembranous ossification [40]. Fávaro-Pípi E, et al. found LIPUS improved bone repair in rats and upregulated BMP4 and RUNX2 expression, particularly in the late stages of recovery [41]. In this model, si-BMP4 injection reduced osteogenic markers and interfered with new bone ingrowth and maturity. BMP4 appears to be a viable approach for the treatment of bone defects and nonunions. BMP4 injection into the medullary cavity of the right femur significantly enhanced osteogenic responses [42]. Furthermore, recombinant human BMP4 (rhBMP-4) was shown to promote new bone formation in rapidly expanding sutures by stimulating ALP activity and upregulating core-binding factor alpha 1 (Cbfa1) and ALP expression [43]. In this study, BMP4 knockdown in vivo attenuated the pro-osteogenic effects of LIPUS, yet LIPUS stimulation partially rescued osteogenesis despite BMP4 silencing, consistent with in vitro findings. These results suggest that BMP4 is crucial for bone formation in PTi, and that LIPUS promotes osteogenesis in part by upregulating BMP4.

Our findings indicate that LIPUS accelerates osteogenesis in PTi by upregulating BMP4 and downregulating miR-1187, establishing BMP4 as a positive regulator of osteogenesis. This study provides a new molecular insight into the mechanism by which LIPUS enhances PTi-induced bone formation, supporting its potential application in CSBD repair. Moreover, BMP4 emerges as a promising therapeutic target for improving the efficacy of LIPUS-PTi co-treatment strategies. However, several limitations of this study should be acknowledged. First, our research primarily focuses on in vitro experiments, and the in vivo validation of these molecular mechanisms remains to be fully explored. Future studies should incorporate animal models to further confirm the osteogenic effects of LIPUS and BMP4 regulation in a physiological environment. Second, while we identified BMP4 as a key regulator, other potential signaling pathways and molecular interactions contributing to LIPUS-induced osteogenesis require further elucidation. Additionally, the optimal parameters of LIPUS stimulation, including intensity, duration, and frequency, need to be systematically investigated to maximize its therapeutic potential. Finally, challenges related to drug delivery, sustained release, and precise control of BMP4 expression must be addressed to translate these findings into clinical applications effectively.

5 | Conclusions

LIPUS promotes osteogenic differentiation of PTi by inhibiting miR-1187 targeted upregulation of BMP4 (Figure 8). This study highlights BMP4 as a key mediator in LIPUS-induced osteogenesis, providing a strong rationale for its therapeutic potential in bone tissue engineering. These findings support the application of LIPUS combined with PTi for treating critical-size bone defects. However, further studies are required to optimize LIPUS parameters, investigate alternative regulatory pathways, and develop efficient drug delivery systems to enhance the clinical applicability of this approach.

Author Contributions

Lin Wu: conceptualization, supervision. **Limei Qin** and **Hongjuan Cao:** methodology, data curation, writing – original draft preparation. **Di Zhang:** visualization, investigation, software. **Lin Wu** and **Xiaohan Liu:** validation, writing – reviewing and editing.

Acknowledgments

The authors have nothing to report.

Ethics Statement

All animal experiments conformed to the guiding principles of the Guide for the Care and Use of Laboratory Animals, and the Animal Ethics Committee of China Medical University approved all experiments (authorization ethics number: CMU2021259).

Consent

All authors approved publication of the manuscript.

Conflicts of Interest

The authors declare no conflicts of interest.

Data Availability Statement

Data available on request due to privacy/ethical restrictions.

References

1. S. Zhao, S. J. Li, W. T. Hou, et al., "Microstructure and Mechanical Properties of Open Cellular Ti-6Al-4 V Prototypes Fabricated by Electron Beam Melting for Biomedical Applications," *Materials and Technologies* 31 (2016): 98–107.

2. Y. B. Li, Y. Z. Liu, H. T. Bai, et al., "Sustained Release of VEGF to Promote Angiogenesis and Osteointegration of Three-Dimensional Printed Biomimetic Titanium Alloy Implants," *Frontiers in Bioengineering and Biotechnology* 9 (2021): 755767.

3. A. Kumar, K. C. Nune, and R. D. K. Misra, "Design and Biological Functionality of a Novel Hybrid Ti-6Al-4 V/Hydrogel System for Reconstruction of Bone Defects," *Tissue Engineering. Part A, Regenerative Medicine* 12, no. 4 (2018): 1133–1144, https://doi.org/10.1002/term.2614.

4. J. Lv, P. Xiu, J. Tan, Z. Jia, H. Cai, and Z. Liu, "Enhanced Angiogenesis and Osteogenesis in Critical Bone Defects by the Controlled Release of BMP-2 and VEGF: Implantation of Electron Beam Melting-Fabricated Porous Ti6Al4V Scaffolds Incorporating Growth Factor-Doped Fibrin Glue," *Biomedical Materials* 10, no. 3 (2015): 035013.

5. H. Zhao, S. Shen, L. Zhao, Y. Xu, Y. Li, and N. Zhuo, "3D Printing of Dual-Cell Delivery Titanium Alloy Scaffolds for Improving Osseointegration Through Enhancing Angiogenesis and Osteogenesis," *BMC Musculoskeletal Disorders* 22, no. 1 (2021): 734.

6. H. Liu, W. Li, C. Liu, et al., "Incorporating Simvastatin/Poloxamer 407 Hydrogel Into 3D-Printed Porous Ti6Al4V Scaffolds for the Promotion of Angiogenesis, Osseointegration and Bone Ingrowth," *Biofabrication* 8, no. 4 (2016): 045012.

7. US Food and Drug Administration (FDA), *Sonic Accelerated Fracture Healing System (SAFHS), Model 2A: Summary of Safety and Effectiveness. Premarket Approval P900009, Exogen Inc* (US Food and Drug Administration, 1994).

8. US Food and Drug Administration (FDA), *Exogen Ultrasound Bone Healing System: Stimulator, Ultrasound and Muscle, for Use Other Than Applying Therapeutic Deep. Premarket Approval P900009/Supplement Number S039* (US Food and Drug Administration, 2015).

9. K. Naruse, A. Miyauchi, M. Itoman, and Y. Mikuni-Takagaki, "Distinct Anabolic Response of Osteoblast to Low-Intensity Pulsed Ultrasound," *Journal of Bone and Mineral Research* 18, no. 2 (2003): 360–369.

10. J. Chen, J. J. Li, F. Hu, et al., "Effect of Microarc Oxidation-Treated Ti6Al4V Scaffold Following Low-Intensity Pulsed Ultrasound Stimulation on Osteogenic Cells In Vitro," *ACS Biomaterials Science & Engineering* 5, no. 2 (2019): 572–581.

11. Y. X. An, Y. Song, Z. L. Wang, et al., "Effect of Low-Intensity Pulsed Ultrasound on the Biological Behaviors of Bone Marrow Mesenchymal Stem Cells on Titanium With Different Surface Topographies," *American Journal of Translational Research* 10, no. 1 (2018): 67–76.

12. V. Carina, V. Costa, L. Raimondi, et al., "Effect of Low-Intensity Pulsed Ultrasound on Osteogenic Human Mesenchymal Stemcells Commitment in a New Bone Scaffold," *Journal of Applied Biomaterials & Functional Materials* 15, no. 3 (2017): e215–e222.

13. L. Feng, X. Liu, H. Cao, L. Qin, W. Hou, and L. Wu, "A Comparison of 1- and 3.2-MHz Low-Intensity Pulsed Ultrasound on Osteogenesis on Porous Titanium Alloy Scaffolds: An In Vitro and In Vivo Study," *Journal of Ultrasound in Medicine* 38, no. 1 (2019): 191–202.

14. H. Cao, L. Feng, Z. Wu, et al., "Effect of Low-Intensity Pulsed Ultrasound on the Biological Behavior of Osteoblasts on Porous Titanium Alloy Scaffolds: An In Vitro and In Vivo Study," *Materials Science & Engineering, C: Materials for Biological Applications* 80 (2017): 7–17.

15. A. A. John, R. Prakash, J. Kureel, and D. Singh, "Identification of Novel microRNA Inhibiting Actin Cytoskeletal Rearrangement Thereby Suppressing Osteoblast Differentiation," *Journal of Molecular Medicine* 96, no. 5 (2018): 427–444.

16. J. Kureel, M. Dixit, A. M. Tyagi, et al., "miR-542-3p Suppresses Osteoblast Cell Proliferation and Differentiation, Targets BMP-7 Signaling and Inhibits Bone Formation," *Cell Death & Disease* 5, no. 2 (2014): e1050.

17. Z. Li, M. Q. Hassan, S. Volinia, et al., "A MicroRNA Signature for a BMP2-Induced Osteoblast Lineage Commitment Program," *Proceedings of the National Academy of Sciences of the United States of America* 105, no. 37 (2008): 13906–13911.

18. D. S. Yu, F. M. An, B. D. Gong, et al., "The Regulatory Role of MicroRNA-1187 in TNF-α-Mediated Hepatocyte Apoptosis in Acute Liver Failure," *International Journal of Molecular Medicine* 29, no. 4 (2012): 663–668.

19. Y. Q. Chen, X. X. Wang, X. M. Yao, et al., "Abated MicroRNA-195 Expression Protected Mesangial Cells From Apoptosis in Early Diabetic Renal Injury in Mice," *Journal of Nephrology* 25, no. 4 (2012): 566–576.

20. L. H. Kung, S. Zaki, V. Ravi, et al., "Utility of Circulating Serum miRNAs as Biomarkers of Early Cartilage Degeneration in Animal Models of Post-Traumatic Osteoarthritis and Inflammatory Arthritis," *Osteoarthritis and Cartilage* 25, no. 3 (2017): 426–434, https://doi.org/10.1016/j.joca.2016.09.002.

21. L. Grgurevic, M. Pecina, S. Vukicevic, et al., "Urist and the Discovery of Bone Morphogenetic Proteins," *International Orthopaedics* 41, no. 5 (2017): 1065–1069.

22. W. Z. Zhuang, X. P. Ge, S. J. Yang, et al., "Upregulation of lncRNA MEG3 Promotes Osteogenic Differentiation of Mesenchymal Stem Cells From Multiple Myeloma Patients by Targeting BMP4 Transcription," *Stem Cells* 33, no. 6 (2015): 1985–1997.

23. Q. Li, S. Q. Zhang, Y. Sui, X. Fu, Y. Li, and S. Wei, "Sequential Stimulation With Different Concentrations of BMP4 Promotes the Differentiation of Human Embryonic Stem Cells Into Dental Epithelium With Potential for Tooth Formation," *Stem Cell Research & Therapy* 10, no. 1 (2019): 276.

24. H. Ochiai, H. Suga, T. Yamada, et al., "BMP4 and FGF Strongly Induce Differentiation of Mouse ES Cells Into Oral Ectoderm," *Stem Cell Research* 15, no. 2 (2015): 290–298.

25. A. Suzuki, T. Takayama, and N. Suzuki, "Daily Low-Intensity Pulsed Ultrasound Stimulates Production of Bone Morphogenetic Protein in ROS 17/2.8 Cells," *Journal of Oral Science* 51, no. 1 (2009): 29–36, https://doi.org/10.2334/josnusd.51.29.

26. Z. L. Zhang, Y. L. Ma, and S. W. Guo, "Low-Intensity Pulsed Ultrasound Stimulation Facilitates In Vitro Osteogenic Differentiation of Human Adipose-Derived Stem Cells via Up-Regulation of Heat Shock Protein (HSP)70, HSP90, and Bone Morphogenetic Protein (BMP) Signaling Pathway," *Bioscience Reports* 38, no. 3 (2018): BSR20180087.

27. National Research Council (US) Committee for the Update of the Guide for the Care and Use of Laboratory Animals, *Guide for the Care and Use of Laboratory Animals* (National Academies Press (US), 2011).

28. G. Q. Liu, Y. L. Guo, L. J. Zhang, et al., "A Standardized Rat Burr Hole Defect Model to Study Maxillofacial Bone Regeneration," *Acta Biomaterialia* 86 (2019): 450–464.

29. S. Rutten, P. A. Nolte, C. M. Korstjens, and J. Klein-Nulend, "Low-Intensity Pulsed Ultrasound Affects RUNX2 Immunopositive Osteogenic Cells in Delayed Clinical Fracture Healing," *Bone* 45 (2009): 862–869.

30. X. Zhou, N. J. Castro, W. Zhu, et al., "Improved Human Bone Marrow Mesenchymal Stem Cell Osteogenesis in 3D Bioprinted Tissue Scaffolds With Low Intensity Pulsed Ultrasound Stimulation," *Scientific Reports* 6 (2016): 32876.

31. J. A. Veronick, F. Assanah, N. Piscopo, et al., "Mechanically Loading Cell/Hydrogel Constructs With Low-Intensity Pulsed Ultrasound for Bone Repair," *Tissue Engineering Part A* 24, no. 3 & 4 (2018): 254–263, https://doi.org/10.1089/ten.tea.2016.0547.

32. M. R. Iaquinta, C. Lanzillotti, C. Mazziotta, et al., "The Role of MicroRNAs in the Osteogenic and Chondrogenic Differentiation of Mesenchymal Stem Cells and Bone Pathologies," *Theranostics* 11 (2021): 6573–6591.

33. B. Zuo, J. F. Zhu, C. D. Wang, et al., "MicroRNA-103a Functions as a Mechanosensitive microRNA to Inhibit Bone Formation Through Targeting Runx2," *Journal of Bone and Mineral Research* 30, no. 2 (2015): 330–345, https://doi.org/10.1002/jbmr.2352.

34. Z. Yang, L. X. Ren, F. Deng, Z. Wang, and J. Song, "Low-Intensity Pulsed Ultrasound Induces Osteogenic Differentiation of Human Periodontal Ligament Cells Through Activation of Bone Morphogenetic Protein-Smad Signaling," *Journal of Ultrasound in Medicine* 33, no. 5 (2014): 865–873.

35. X. D. Lu, W. X. Han, and Y. X. Liu, "Suppression of miR▪451a Accelerates Osteogenic Differentiation and Inhibits Bone Loss via Bmp6 Signaling During Osteoporosis," *Biomedicine & Pharmacotherapy* 120 (2019): 109378.

36. Y. J. Cao, Q. X. Lv, and C. T. Lv, "MicroRNA-153 Suppresses the Osteogenic Differentiation of Human Mesenchymal Stem Cells by Targeting Bone Morphogenetic Protein Receptor Type II," *International Journal of Molecular Medicine* 36, no. 3 (2015): 760–766, https://doi.org/10.3892/ijmm.2015.2275.

37. S. Manaka, N. Tanabe, T. Kariya, et al., "Low-Intensity Pulsed Ultrasound-Induced ATP Increases Bone Formation via the P2X7 Receptor in Osteoblast-Like MC3T3-E1 Cells," *FEBS Letters* 589, no. 3 (2015): 310–318.

38. A. P. Hensley and A. McAlinden, "The Role of microRNAs in Bone Development," *Bone* 143 (2021): 115760.

39. S. L. Wu, Y. Kawahara, T. Manabe, et al., "Low-Intensity Pulsed Ultrasound Accelerates Osteoblast Differentiation and Promotes Bone Formation in an Osteoporosis Rat Model," *Pathobiology* 76, no. 3 (2009): 99–107.

40. D. Volarić, G. Žauhar, and J. Chen, "The Effect of Low-Intensity Pulsed Ultrasound on Bone Regeneration and the Expression of Osterix and Cyclooxygenase-2 During Critical-Size Bone Defect Repair," *International Journal of Molecular Sciences* 25, no. 7 (2024): 3882, https://doi.org/10.3390/ijms25073882.

41. E. Fávaro-Pípi, P. Bossoni, P. D. Oliveira, et al., "Low-Intensity Pulsed Ultrasound Produced an Increase of Osteogenic Genes Expression During the Process of Bone Healing in Rats," *Ultrasound in Medicine & Biology* 36, no. 12 (2010): 2057–2064.

42. Y. Shiozaki, T. Kitajima, T. Mazaki, et al., "Enhanced In Vivo Osteogenesis by Nanocarrier-Fused Bone Morphogenetic Protein-4," *International Journal of Nanomedicine* 8 (2013): 1349–1360.

43. Q. R. Shen, S. S. Zhu, J. Hu, N. Geng, and S. Zou, "Recombinant Human Bone Morphogenetic Protein-4 (BMP-4)-Stimulated Cell Differentiation and Bone Formation Within the Expanding Calvarial Suture in Rats," *Journal of Craniofacial Surgery* 20, no. 5 (2009): 1561–1565.

Supporting Information

Additional supporting information can be found online in the Supporting Information section.